Virtual Landmarks

Yubing Tong, Jayaram K. Udupa, Dewey Odhner, Peirui Bai, Drew A. Torigian

Medical Image Processing Group, 602 Goddard building, 3710 Hamilton Walk, Department of Radiology, University of Pennsylvania, Philadelphia, PA 19104 United States

ABSTRACT

Much has been published on finding landmarks *on* object surfaces in the context of shape modeling. While this is still an open problem, many of the challenges of past approaches can be overcome by removing the restriction that landmarks *must be* on the object surface. The *virtual landmarks* we propose may reside inside, on the boundary of, or outside the object and are tethered to the object. Our solution is straightforward, simple, and recursive in nature, proceeding from global features initially to local features in later levels to detect landmarks. Principal component analysis (PCA) is used as an engine to recursively subdivide the object region. The object itself may be represented in binary or fuzzy form or with gray values. The method is illustrated in 3D space (although it generalizes readily to spaces of any dimensionality) on four objects (liver, trachea and bronchi, and outer boundaries of left and right lungs along pleura) derived from 5 patient computed tomography (CT) image data sets of the thorax and abdomen. The virtual landmark identification approach seems to work well on different structures in different subjects and seems to detect landmarks that are homologously located in different samples of the same object. The approach guarantees that virtual landmarks are invariant to translation, scaling, and rotation of the object/image. Landmarking techniques are fundamental for many computer vision and image processing applications, and we are currently exploring the use virtual landmarks in automatic anatomy recognition and object analytics.

Keywords: Virtual landmarks, Principal Component Analysis (PCA), image segmentation, shape.

1. INTRODUCTION

Landmark-based techniques have been widely used in the computer vision and image processing fields, especially in medical image segmentation, registration, and shape analysis. Landmarks can be identified in purely manual or automatic ways. Some anatomic locations, such as the aortic root or the inferior aspect of the mandible, can be manually labeled as landmarks [1-3]. However, labeling landmarks manually is tedious, and may lead to low repeatability, especially when labeling a point/voxel in 3D space on slices or on 3D surfaces. An automatic landmark-defining program can be devised based on machine learning techniques to initially set up landmarks, followed by another operation such as non-rigid registration to refine the correspondence between landmarks [4-6]. These approaches are indirect and involve higher complexity derived from non-rigid registration. Much has been published on finding landmarks *on* object surfaces in the context of shape modeling. While this is still an open problem, many of the challenges of past approaches can be overcome by removing the restriction that landmarks must be on the object surface. The *virtual landmarks* we propose may reside inside, on the boundary of, or outside the object and are tethered to the object. Our goal for virtual landmarks is simply to describe accurately positions relative to the object. Our solution is straightforward, simple, and recursive in nature, proceeding from global features initially to local features in later levels to detect landmarks. Principal component analysis (PCA) is used as an engine to recursively subdivide the object. The method is illustrated in 3D space, but it generalizes readily to any K-dimensional space and can be utilized in any landmark-related applications of computer vision and pattern recognition.

Generally, the main contribution of this paper is to propose a novel PCA-based automatic landmark identification approach in which landmarks are not constrained to lie on object surfaces. Then, the approach is demonstrated to be able

Medical Imaging 2017: Image-Guided Procedures, Robotic Interventions, and Modeling, edited by Robert J. Webster III, Baowei Fei, Proc. of SPIE Vol. 10135, 1013521 · © 2017 SPIE
CCC code: 1605-7422/17/$18 · doi: 10.1117/12.2254855

to work well on different subjects and different anatomic structures and on both binary and gray object representations. Finally, empirical demonstration is made to show the theoretical property that the landmarks detected are invariant to rigid transformations.

2. MATERIALS & METHODS

2.1 Image data

Thoracic and abdominal CT images from 5 near normal subjects are utilized in our experiments. As in our previous studies, all CT images were selected from our health system patient image database following approval from the Institutional Review Board at the Hospital of the University of Pennsylvania along with a Health Insurance Portability and Accountability Act waiver. In this study, 4 objects including liver, trachea & bronchi (tb), the outer boundary of the left lung along the left pleura (lps), and the outer boundary of the right lung along the right pleura (rps) from diagnostic contrast-enhanced CT (with a voxel size of $0.72 \times 0.72 \times 5$ mm^3) are utilized to illustrate virtual landmark properties. The whole-body skeleton from a low-dose unenhanced CT scan (with a voxel size of $1.17 \times 1.17 \times 4$ mm^3) is also used to calculate virtual landmarks and to visualize them in the whole body.

2.2 Virtual landmarks

Principal component analysis (*PCA*)

PCA [7] is a commonly-used statistical pattern recognition procedure that employs an orthogonal transformation to convert a set of observations of possibly correlated random variables into a set of linearly uncorrelated random variables called principal components. Roughly speaking, the eigenvalues resulting from applying this analysis to the points in a 3D object region indicate the variance (dispersion) of the object points in the three directions represented by the corresponding eigenvectors. The largest eigenvector indicates the direction of elongation of the object and the other two eigenvectors indicate roughly the directions of breadth and thickness of the object.

Iterative PCA based virtual landmark identification

The idea underlying the concept of *virtual landmarks* of an object is illustrated with a 2D example in Figure 1. Given a binary image representing the object, PCA of the entire binary 2D object region is first carried out to find the four principal axes directions, denoted in the figure in green by $A_{1,1}$, $A_{1,2}$, $A_{1,3}$, $A_{1,4}$, emanating from the geometric centroid of the object. Along these axes, we find points $P_{1,1}$, $P_{1,2}$, $P_{1,3}$, and $P_{1,4}$ that indicate the extent of the object in those directions. These four points together with the geometric center form the first level landmarks (first subscript denotes level). These points and the axes subdivide the shape into four pieces in the four (not necessarily equal) quadrants. For each piece, we perform PCA again and find the 16 second level landmarks denoted $P_{2,1}$, $P_{2,2}$, …, $P_{2,16}$ and the 4 geometric centers. The four points $P_{2,13}$, $P_{2,14}$, $P_{2,15}$, and $P_{2,16}$ obtained for the 4th quadrant and the corresponding geometric center are shown in the figure for illustration (2nd level principal axes are shown in red). The process continues up to a specified level. Note that the points are ordered and hence have unique labels. This allows us to specify the landmarks we need by their labels for representing a given shape. For our example, we may use just the 7 points $P_{1,1}$, $P_{1,2}$, $P_{1,3}$, $P_{1,4}$, $P_{2,13}$, $P_{2,14}$, and $P_{2,16}$ (which already denote the shape roughly). Different objects may be codified by different numbers of points. Note how the points tend to move closer to the object surface at higher levels. In the 3D case, at level n, we will have 8^{n-1} octants and there will be in total $7\sum_{x=1}^{n} 8^{x-1}$ points for n levels. The total number of virtual landmarks for 1, 2, and 3 levels are 7, 63, and 511, respectively. Landmarks at early levels capture overall form whereas points at later levels provide more subtle details of form. Note that the above expression gives the maximum number of virtual landmarks for a given number of levels. In a given shape, empty octants at any given level and beyond will not contribute any landmarks.

Unlike methods of finding landmarks on boundaries, this approach generalizes to spaces of any finite dimension easily. For *K*-dimensional space, the maximum total number of points for n levels will be $(2K+1)\sum_{x=1}^{n} 2^{K(x-1)}$. From the definition and the iterative PCA procedure, it is easy to demonstrate that the derived landmarks are invariant to translation, rotation, and (uniform) scaling of the binary object. The method also readily generalizes to non-binary

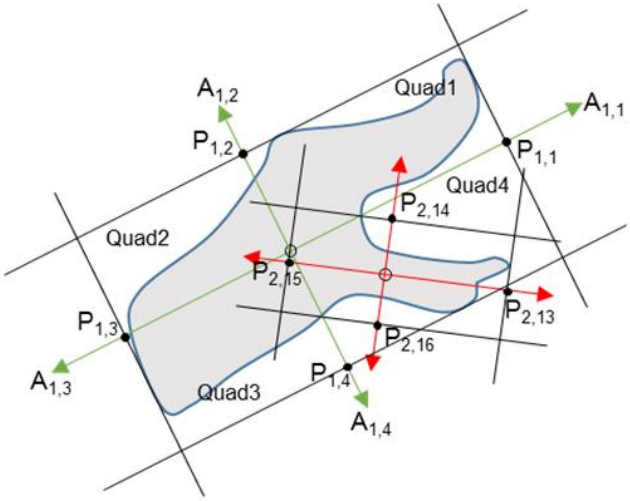

Figure 1. The illustration of landmarks from iterative PCA on a 2D object.

objects – fuzzy objects and objects with gray values defined for their voxels – by considering the "weight" of the individual voxels within the object in performing PCA.

3. RESULTS

3.1 Virtual landmarks of different objects

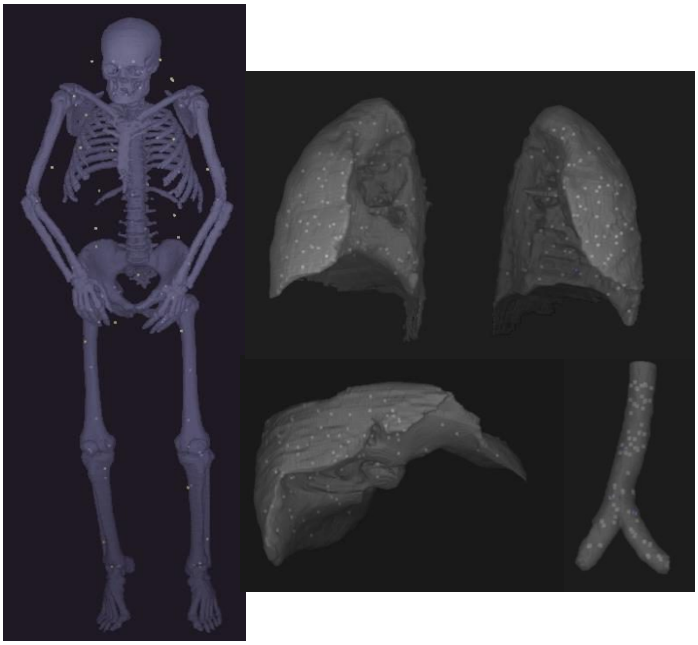

Figure 2. Virtual landmarks of skeleton, rps, lps, liver, and tb derived from image data from one subject.

Figure 2 shows the virtual landmarks derived for different objects: whole-body skeleton, rps, lps, liver, and tb, where landmarks in 3D space are overlaid on to those objects' 3D surface renditions. In all examples shown, landmarks up to

the third level and only those landmarks representing the geometric centers are demonstrated. The virtual landmarks seem to be distributed through whole objects more-or-less uniformly, meaning that they are not concentrated all in one portion of the object. Note also how the landmarks may lie anywhere in space.

Many landmarks may not be on the surface of objects, especially for the skeleton. In fact, it is rare to find a landmark precisely on the object's surface. Placement exactly on the surface can happen only when an eigenvector intersects the surface precisely at a point which is also the tangent point to a plane drawn orthogonal to the eigenvector. The landmarks, even when outside or inside the object, still have a strong connection with the target structure. That is why they are named *virtual landmarks*. From Figure 2 we can see that the concept of virtual landmarks seems to apply equally well to different objects. Interestingly, some points at the junction of the bronchi are also selected by the approach as virtual landmarks.

3.2 Virtual landmarks from different subjects

Figure 3 shows the virtual landmarks of tb and lps, each set derived from 5 subjects. Observe that the virtual landmarks from these different subjects follow a similar pattern, which preliminarily demonstrates that the landmarks are detected at homologous locations in different samples of the same object from different subjects. This will form the fundamental basis for applications based on virtual landmarks, such as building object models or locating objects automatically on images, etc. In other words, virtual landmarks seem to be able to encapsulate the intrinsic shape properties of objects.

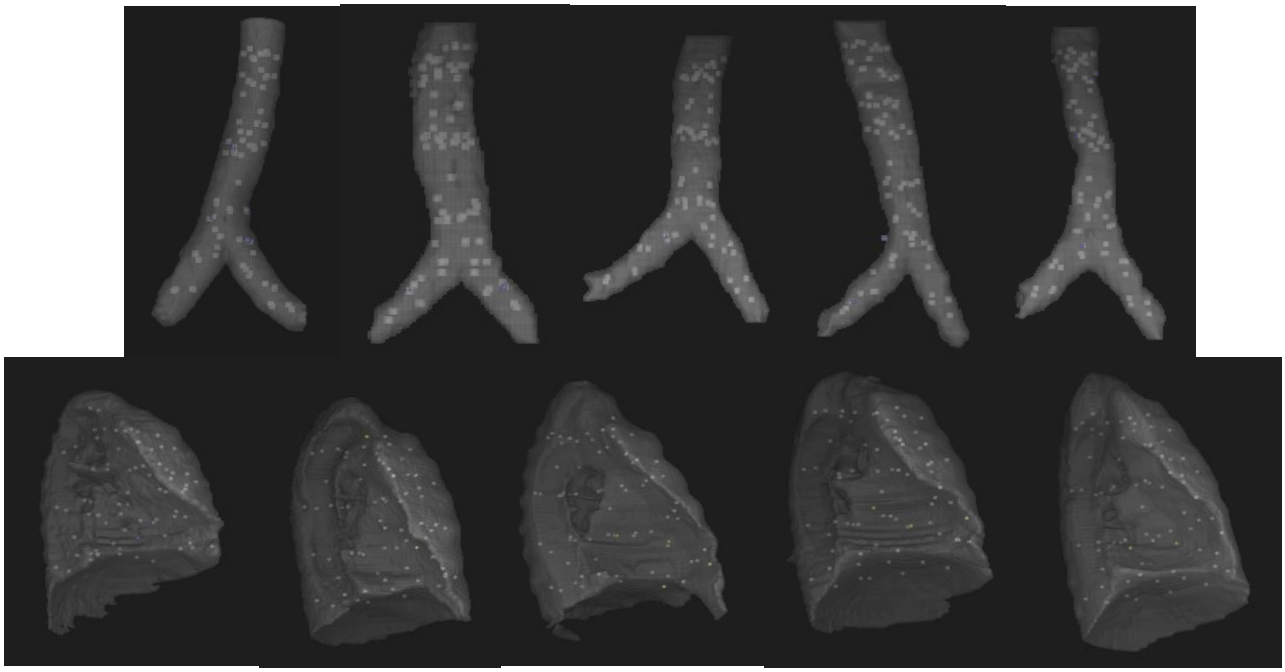

Figure 3. Virtual landmarks of tb and lps in five patients.

3.3 Virtual landmarks after translation, scaling, and rotation

Five thoracic CT images as well as their binary masks were translated (10 mm in x and y direction), scaled in x, y and z direction by a factor of 1.2, and rotated by 90 degrees with respect to the original image for all four objects. The virtual landmarks were computed and the Euclidian distance among virtual landmarks before and after the transformation was computed (Table 1). The average distance (error) is a fraction of the pixel size (which is 0.72 mm), stemming mostly from interpolation errors. This empirically demonstrates that the virtual landmarks are invariant to rigid transformations of the image/objects. This, we believe, is a useful theoretical property of the approach in landmark-based applications.

Table 1. Mean (sd) distance (in mm) between virtual landmarks from objects before and after rigid transformation.		
Translation	Scaling	Rotation
0.22 (0)	0.24 (0.22)	0.61 (0.15)

3.4 Virtual landmarks on binary versus gray images

As mentioned earlier, virtual landmarks can be derived from the object binary mask or from the corresponding intensity image. The landmarks derived from these two methods may differ depending on the pattern of intensity distribution within the object. Table 2 shows the Euclidian distance (the average and standard deviation) between corresponding landmarks derived from those two methods for different objects.

Table 2. Mean (sd) of distances (in mm) between virtual landmarks derived from binary and gray images for liver, tb, lps, and rps.			
liver	tb	lps	rps
0.29 (0.21)	7.18 (3.94)	18.61 (10.19)	21.85 (15.28)

Considering the fact that slice separation is 5mm in these data sets, the average distance for landmarks of liver and tb is around 1 voxel, implying that the virtual landmarks of liver and tb derived from binary and gray images are almost the same. However, these distances for lps and rps are larger. The reason is the larger degree of non-uniformity of image intensities inside these objects. Figure 4 shows the binary masks of liver, tb, lps, and rps overlaid on gray image slices for one subject. The intensity inside the liver mask is more uniform than the intensities of lps and rps. Virtual landmarks for liver from binary image and gray image are much similar to each other comparing with other three objects, tb, rps, and lps. In general, virtual landmarks generated by the two methods can be quite different, especially at higher levels of subdivision.

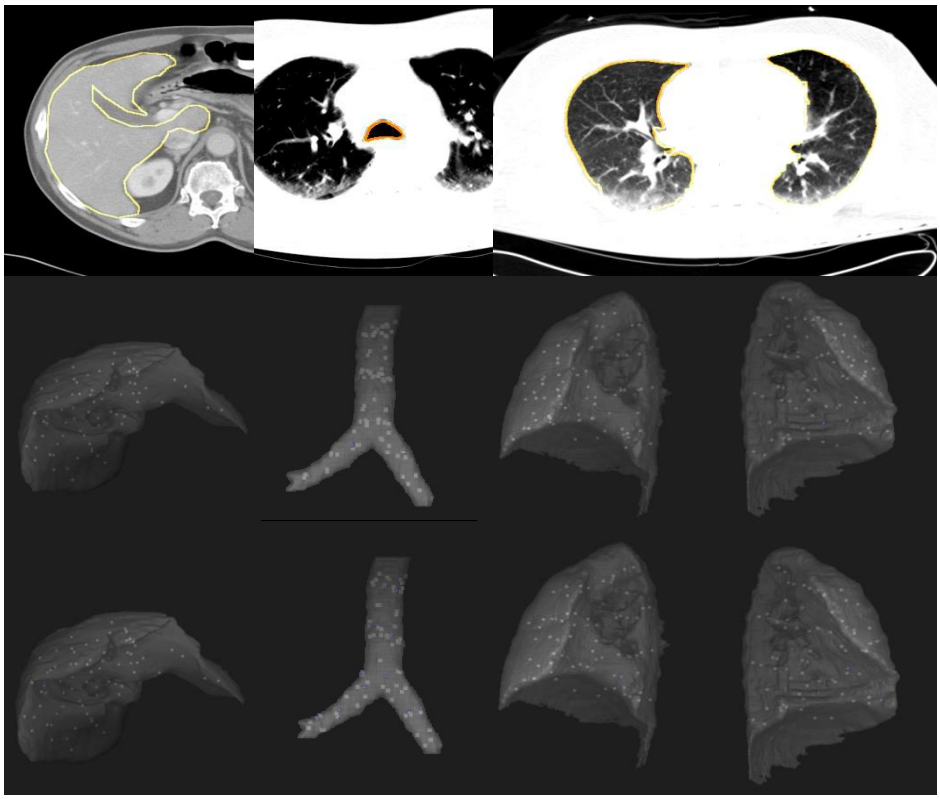

Figure 4. Binary masks (in color) for liver, tb, rps and lps on the top row. Virtual landmarks from the binary images are at the middle row. And virtual landmarks from gray images are at the bottom row.

4. CONCLUSIONS

This paper introduces a novel PCA-based automatic landmark identification approach which automatically resolves the issue of establishing homology among landmarks from different object samples. Previous approaches to landmark identification consisted of two disparate steps of first detecting landmarks and then finding homology. In the virtual landmark approach, the concept of homology is built into the definition of the landmarks. The method removes the restriction of past approaches which require the landmarks to be situated on the object surface and allows them to be anywhere with respect to the object, although they remain tethered to the object by its shape and/or intensity distribution. The approach guarantees that virtual landmarks are invariant to rigid transformations. The virtual landmarks seem to be tagged at homologous locations in the same object derived from different subject image data sets.

One application of virtual landmarks is to automatically localize anatomic body regions with the idea that the geometric relationship between these landmarks of reference objects and the boundary locations of body regions can be learned through a neural network regressor, and then the locations can be predicted. More details can be found in Reference [8] which is a separate paper presented at this SPIE Medical Imaging 2017 conference. Clearly, virtual landmarks can be readily used for active shape and active appearance modeling, where finding homologous landmarks has remained an open problem. Further exploration of the properties and applications of virtual landmarks, particularly for automatic anatomy recognition, constitutes some of our on-going and future works.

REFERENCES

[1] Elattar M, Wiegerinck E, van Kesteren F, Dubois L, Planken N, Vanbavel E, Baan J, Marquering H., "Automatic aortic root landmark detection in CTA images for preprocedural planning of transcatheter aortic valve implantation," Int J Cardiovasc Imaging. 32(3), 501-511 (2016).

[2] Zheng Y, John M, Liao R, Nottling A, Boese J, Kempfert J, Walther T, Brockmann G, Comaniciu D., "Automatic aorta segmentation and valve landmark detection in C-arm CT for transcatheter aortic valve implantation," IEEE Trans Med Imaging. 31(12),2307-2321 (2012).

[3] Gupta A, Kharbanda OP, Sardana V, Balachandran R, Sardana HK., "Accuracy of 3D cephalometric measurements based on an automatic knowledge-based landmark detection algorithm," Int J Comput Assist Radiol Surg. 11(7), 1297-1309 (2016).

[4] Juneja A, Espy-Wilson C., "A probabilistic framework for landmark detection based on phonetic features for automatic speech recognition," J Acoust Soc Am. 123(2):1154-1168 (2008).

[5] Heimann T, Wolf I, Meinzer HP., "Automatic generation of 3D statistical shape models with optimal landmark distributions," Methods Inf Med. 46(3), 275-281 (2007).

[6] Cheng E, Chen J, Yang J, Deng H, Wu Y, Megalooikonomou V, Gable B, Ling H., "Automatic Dent-landmark detection in 3-D CBCT dental volumes," Conf Proc IEEE Eng Med Biol Soc. 6204-6207 (2011).

[7] Sonka M, Hlavac V, Boyle R. [Image Processing, Analysis, and Machine Vision], Cengage Learning, 74-77. 4th ed., 2015. ISBN-13: 978-133-59360-7.

[8] Bai PR, Udupa JK, Tong YB, Xie SP, Torigian, DA., "Automatic body region localization", SPIE, Medical Imaging 2017, 10134-139.